

Article

Effect of Permeability Anisotropy on the Production of Multi-Scale Shale Gas Reservoirs

Ting Huang ^{1,*}, Zhengwu Tao ², Erpeng Li ², Qiqi Lyu ¹ and Xiao Guo ³

¹ Hubei Cooperative Innovation Center of Unconventional Oil and Gas, Yangtze University, Wuhan 430100, China; qiqi_lyu@hotmail.com

² Tarim Oilfield Company, PetroChina, Korla, Xinjiang 841000, China; taozw-tlm@petrochina.com.cn (Z.T.); lierpeng-tlm@petrochina.com.cn (E.L.)

³ State Key Laboratory of Oil and Gas Reservoir Geology and Exploitation, Southwest Petroleum University, Chengdu 610500, China; guoxiao72@163.com

* Correspondence: huang331@yangtzeu.edu.cn

Received: 6 August 2017; Accepted: 29 September 2017; Published: 9 October 2017

Abstract: Shales or mudstones are fine grained and layered reservoirs, which leads to strong shale permeability anisotropy. Shale has a wide pore-size distribution, and pores with different diameters contribute differently to the apparent permeability of shales. Therefore, understanding the anisotropy of multiscale shale gas reservoirs is an important aspect to model and evaluate gas production from shales. In this paper, a novel model of permeability anisotropy for shale gas reservoirs is presented to calculate the permeability in an arbitrary direction in three dimensional space. A numerical model which is valid for the entire Knudsen's range (continuum flow, slip flow, transition flow and free molecular flow) in shale gas reservoirs was developed, and the effect of gas-water flow and the simulation of hydraulic fracturing cracks were taken into consideration as well. The simulation result of the developed model was validated with field data. Effects of critical factors such as permeability anisotropy, relative permeability curves with different nanopore radii and initial water saturation in formation on the gas production rate of multi-stage fractured horizontal well were discussed. Besides, flow regimes of gas flow in shales were classified by Knudsen number, and the effect of various flow regimes on both apparent permeability of shales and then the gas production has been analyzed thoroughly.

Keywords: shale gas; anisotropy; multiscale flow; gas-water flow; multi-stage fractured horizontal well

1. Introduction

Shales or mudstones are fine grained and layered reservoirs [1], which leads to strong shale permeability anisotropy. The range of pore diameter distributions is large in actual shales, so gas flow in shales undergoes a transition from a Darcy regime to other regimes owing to the significant effect of collisions between molecules and pore walls on gas transport [2]. Therefore, considerable efforts should be undertaken to improve the knowledge of the physics behind gas flow in multiscale shale gas reservoirs with permeability anisotropy.

The anisotropy of shale was reported early by Young et al. [3]. Different composition and compaction history make shale reservoir anisotropic, so understanding the anisotropy of shale reservoirs is an important aspect to model and evaluate gas production from shales. Some researchers have studied the permeability anisotropy of shales. Kwon et al. [4] reported that the permeabilities of Wilcox shale measured parallel to bedding are about one order of magnitude greater than those measured perpendicular to bedding. Other researchers mainly focused on seismic or log data [5–7],

anisotropy of elastic properties or clay mineral alignment [8,9]. Nevertheless, little work has been done to investigate the effect of anisotropy of shales on gas production.

Shales consist of large amounts of nanopores, a certain number of micropores and microfractures. Gas transfer in nanopores is a complex process under the effects of pore diffusion, surface diffusion, slip flow and gas desorption [10–13]. Numerical models which consider Knudsen diffusion, slip flow and gas desorption in nanopores for shale gas reservoirs have been analyzed by many researchers [14–17], but the pore structure in shale is complex because of its wide pore-size distribution, so Knudsen diffusion and slippage effect in nanopores cannot be used to describe all the flow regimes in multiscale pores. Knudsen number is used to classify the flow regimes in shales [18], and Beskok and Karniadakis [19] developed a rigorous equation which is applicable for the entire Knudsen range to account for all flow regimes including continuum flow, slip flow, transition flow and molecular flow. Ziarani and Aguilera [18] used the Beskok-Karniadakis equation to correct the permeability of shales and their model was validated with data from the Mesaverde formation in the U.S. Civan et al. [20] used the Beskok-Karniadakis equation to determine the relationship between the intrinsic permeability and apparent permeability. Wang et al. [21] presented the apparent permeability for gas transport in nanopores of shale gas reservoirs based on the Beskok-Karniadakis equation. Yuan et al. [22] used the Beskok-Karniadakis equation to build an analytical model of apparent gas permeability for tight porous media.

Moreover, economic production of unconventional resources relies heavily on advanced completion technology such as horizontal wells with multi-stage hydraulic fracture stimulations. In terms of the research on rate transient analysis of multi-fractured horizontal wells, an analytical trilinear flow model was developed to study the transient behavior of fractured wells [14,23]. In addition, semi-analytical model based on Green's function and the source/sink method was presented to facilitate transient pressure/rate for fractured well [24,25]. However, many simplification assumptions are needed to solve the analytical or semi-analytical solution for shale gas reservoirs with complex storage and seepage mechanisms, which are not fully built on the real physical model compared with numerical models, so the performance of multi-fractured horizontal wells has been modeled by many researchers [26–28] through numerical simulation methods or using commercial software.

Little work however has been done in the previous literature to simultaneously incorporate permeability anisotropy in multiscale shale gas reservoir, and the simulation of multi-fractured horizontal wells in numerical models for shale gas reservoirs. In this paper, a comprehensive multiscale model is established, which considers permeability anisotropy of shales, different flow regimes in shale, gas-water flow in formation and the advanced completion technology of multi-stage fractured horizontal wells. The simulation results have been validated with actual field data, and the effects of shale anisotropy, non-Darcy flow effect in multiscale shales, gas-water flow and hydraulic fractures on the gas production rate of multi-fractured horizontal wells were analyzed thoroughly.

2. Calculation Model of Permeability Anisotropy for Shale Gas Reservoirs

Research and practice show that permeabilities are not the same in different directions, so permeability has vector characters. The vector property of permeability will affect the design of well placement, well spacing and hydraulic fracture treatments. However, there exist some confused understandings in comprehending and applying the vector property of permeability (see Appendix A), so a novel model is proposed in this paper to calculate permeability in any direction in three dimensional space.

In real anisotropic formation, the bedding plane is not necessarily parallel to the horizontal plane, but has an angle with the horizontal plane (Figure 1), so a model for calculating permeability in any direction in three dimensional space is developed, which considers the dip and azimuth. α is defined as the angle between the bedding plane and the horizontal plane, and β is defined as the angle between the arbitrary direction and the east direction in the clockwise direction.

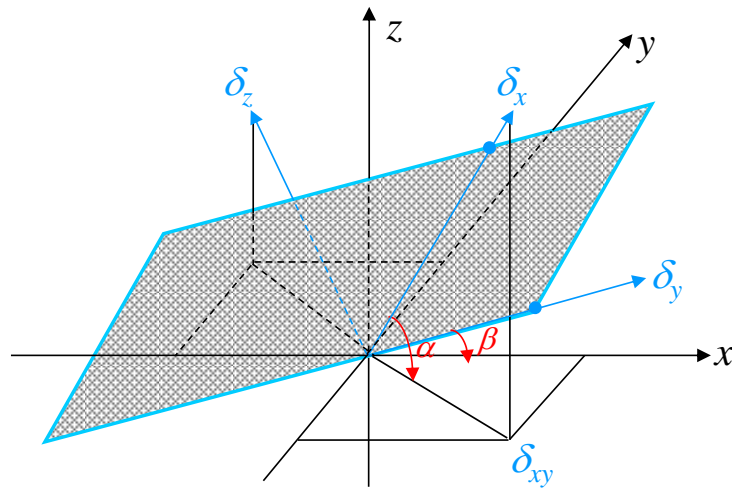


Figure 1. Schematic of calculation model considering dip and azimuth.

We first calculate k_z (permeability in z direction) and $k_{\delta xy}$ (in the horizontal plane), as $k_{\delta x}$ and $k_{\delta z}$ are known parameters which can be obtained in the laboratory. Because the directions of k_z , $k_{\delta xy}$, $k_{\delta x}$ and $k_{\delta z}$ are all in the same plane, so we can apply the results of our model to calculate permeability in an arbitrary direction in two dimensional space (see Appendix A):

$$k_{\delta xy} = k_{\delta x} \cos^2 \alpha + k_{\delta z} \sin^2 \alpha \quad (1)$$

$$k_z = k_{\delta x} \sin^2 \alpha + k_{\delta z} \cos^2 \alpha \quad (2)$$

Then k_x and k_y can be obtained in the same way (k_x , k_y , $k_{\delta y}$ and $k_{\delta xy}$ are all in the horizontal plane), as $k_{\delta y}$ is a known parameter and $k_{\delta xy}$ can be calculated by Equation (1):

$$k_x = k_{\delta x} \cos^2 \alpha \cos^2 \beta + k_{\delta y} \sin^2 \beta + k_{\delta z} \sin^2 \alpha \cos^2 \beta \quad (3)$$

$$k_y = k_{\delta x} \cos^2 \alpha \sin^2 \beta + k_{\delta y} \cos^2 \beta + k_{\delta z} \sin^2 \alpha \sin^2 \beta \quad (4)$$

When dip α is equal to 0, this three-dimensional calculation model should be simplified to two dimensional calculation model presented in Appendix A. Equations (3) and (4) can be simplified to Equations (A10) and (A11), respectively, when α is equal to 0, which demonstrates the validity of our model. Therefore, the permeability of anisotropy reservoir can be written in the form of a vector:

$$\vec{K} = (k_x, k_y, k_z) = (k_{\delta x}, k_{\delta y}, k_{\delta z}) \begin{bmatrix} \cos^2 \alpha \cos^2 \beta & \cos^2 \alpha \sin^2 \beta & \sin^2 \alpha \\ \sin^2 \beta & \cos^2 \beta & 0 \\ \sin^2 \alpha \cos^2 \beta & \sin^2 \alpha \sin^2 \beta & \cos^2 \alpha \end{bmatrix} \quad (5)$$

3. Multi-Scale Seepage Non-Linear Model in Shale Gas Reservoirs

3.1. Knudsen Number and Multi-Scale Flow Regimes in Shale Gas Reservoirs

Besides permeability anisotropy, shales consist of large amounts of nanoscale pores (pore radius: 5–900 nm), a certain number of microscale pores (pore radius: 12–800 μm) and microfractures (Figure 2). In microscale pores, Darcy flow is the dominant flow transport mechanism; however, when the pore radius is as small as a few nanometers, diffusion plays an important role which must be considered. Conventional Darcy equation cannot fully capture the physics of flow in the nanopores of shales, and gas flow in nanoscale pores must consider the submicron effects such as diffusion and slippage, so pores with different diameters contribute differently to gas flow, and a rigorous approach is needed to describe gas flow in multiscale shales.

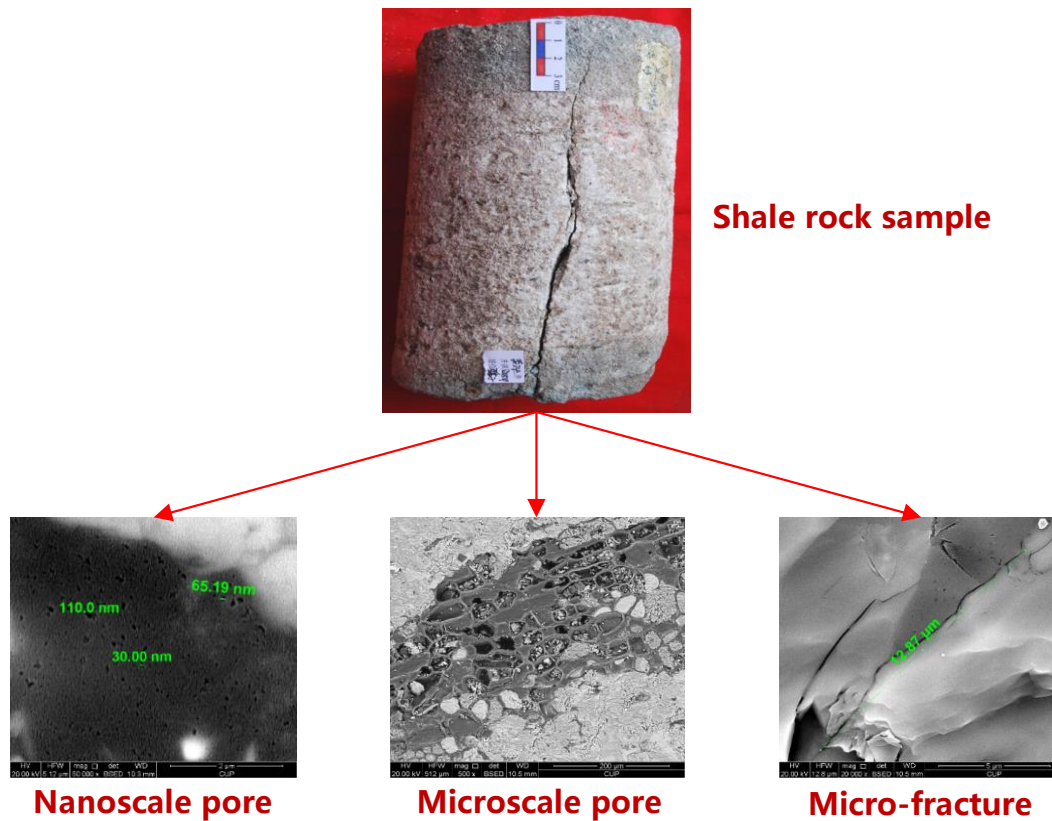


Figure 2. Microscopic pore structure of shales.

The Knudsen number Kn is defined as the ratio of molecular mean free path λ and pore radius r , which is a widely recognized dimensionless parameter to determine the degree of appropriateness of continuum model:

$$Kn = \frac{\lambda}{r} \tag{6}$$

Gas flow regimes can be classified into four categories [10] based on Knudsen number (Table 1): (1) continuum flow; (2) slip flow; (3) transition flow; (4) free-molecule flow. In continuum flow regime, the no-slip boundary condition is valid, and gas flow is linear. As Knudsen number increases, the rarefaction effects become more significant, and the continuum assumption breaks down eventually, so for flow regimes other than continuum flow, the traditional equation of Darcy’s law is not applicable anymore.

Table 1. Classification of gas flow regimes based on Knudsen number.

Knudsen Number	$Kn \leq 0.001$	$0.001 < Kn \leq 0.1$	$0.1 < Kn \leq 10$	$Kn > 10$
Flow regime	Continuum flow	Slip flow	Transition flow	Free-molecule flow

To analyze the flow regimes in shale gas reservoirs, Figure 3 presents the Knudsen number under different pore sizes between 1 nm and 500 μm and different pressure ranging from atmospheric pressure to 100 MPa. Knudsen number increases when pressure drops and pore throat diameter decreases. As illustrated in Figure 3, we can find that gas flow in microscale pores and micro-fracture (pore radius > 10 μm) is mainly continuum flow, which can be presented by Darcy formula as same as gas flow in conventional reservoir. However, when pore radius decreases from microscale to nanoscale, gas flow undergoes a transition from Darcy regime to slip flow and transition flow. Only when the pressure is below 1 MPa and pore radius is about 1 nm, will the gas flow in shale gas reservoir be

free-molecule flow. Thus, we can conclude that gas flow in shale gas reservoirs is a multi-scale flow process mainly including continuum flow, slip flow and transition flow.

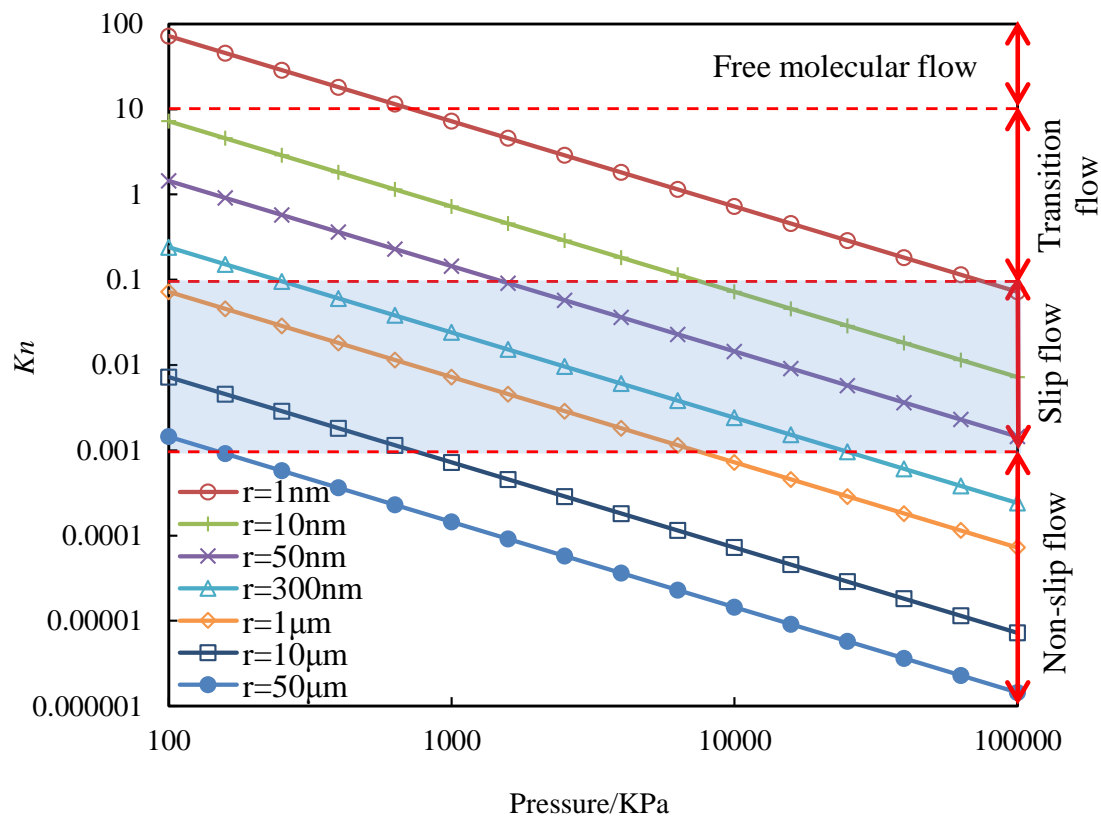


Figure 3. Knudsen number under different pressure and pore radii.

3.2. Apparent Permeability Model Valid for Different Flow Regimes

A transport model valid for the entire Knudsen’s range (continuum flow, slip flow, transition flow and free-molecule flow) is given below, which considers viscous flow, Knudsen diffusion and slip flow [19,29]:

$$v = -\frac{K_\infty}{\mu} (1 + \alpha_r Kn) \left(1 + \frac{4Kn}{1 - bKn} \right) \frac{dp}{dx} \tag{7}$$

So the apparent permeability and permeability correction factor can be defined as:

$$K_a = K_\infty f(Kn) \tag{8}$$

$$f(Kn) = [1 + \alpha_r(Kn)Kn] \left(1 + \frac{4Kn}{1 - bKn} \right) \tag{9}$$

We can see from Equation (8) to Equation (9), that the apparent permeability is nearly equal to the absolute permeability when Kn approaches 0; When the Knudsen number gets bigger, it means flow in pores is no longer Darcy flow and the apparent permeability should be corrected.

The rarefaction coefficient is given by Beskok and Karniadakis [19]:

$$\alpha_r(Kn) = \frac{128}{15\pi^2} \tan^{-1} (4Kn^{0.4}) \tag{10}$$

Knudsen number is defined as the ratio of the molecular mean free path and equivalent hydraulic radius, which can be expressed as:

$$Kn = \frac{\lambda}{r_h} = \frac{\mu}{p_g r_h} \sqrt{\frac{\pi RT}{2M}} \quad (11)$$

The gas compressibility factor is calculated by the following equation [30]:

$$Z = 1 + \frac{p_r}{10.24 T_r} \left[2.16 \frac{1}{T_r} \left(\frac{1}{T_r} + 1 \right) - 1 \right]$$

$$p_r = p/p_c \quad (12)$$

$$T_r = T/T_c$$

The viscosity of real gas is calculated by [30]:

$$\mu_r = \mu \left[1 + \frac{A_1}{T_r^5} \left(\frac{p_r^4}{T_r^{20} + p_r^4} \right) + A_2 \left(\frac{p_r}{T_r} \right)^2 + A_3 \left(\frac{p_r}{T_r} \right) \right] \quad (13)$$

The Knudsen number of real gas through nanopores is obtained as:

$$Kn_r = \frac{\lambda_r}{r_h} = \frac{\mu_r}{p_g r_h} \sqrt{\frac{\pi ZRT}{2M}} \quad (14)$$

so Equation (9) can be rewritten as:

$$f(Kn_r) = \left[1 + \alpha_r \left(\frac{\mu_r}{p_g r_h} \sqrt{\frac{\pi ZRT}{2M}} \right) \frac{\mu_r}{p_g r_h} \sqrt{\frac{\pi ZRT}{2M}} \right] \left(1 + \frac{4 \frac{\mu_r}{p_g r_h} \sqrt{\frac{\pi ZRT}{2M}}}{1 - b \frac{\mu_r}{p_g r_h} \sqrt{\frac{\pi ZRT}{2M}}} \right) \quad (15)$$

Figure 4a shows how the permeability correction factor varies with pressure under different pore radii. The higher the pressure is, the lower the correction factor is. When the pressure is higher than 10 MPa and the pore radius is larger than 0.1 μm , the correction factor can be negligible. In addition, the permeability correction factor becomes larger and more evident as the pore radius becomes smaller, so pores with different radii contribute differently to the apparent permeability of shales. As illustrated in Figure 4a, we can also find that real gas effect should be considered to model Knudsen number at a high pressure.

Figure 4b shows how permeability correction factor varies with Knudsen number and pore radius, which illustrates typical flow regimes and the corresponding permeability correction factors of a given pore radius. The range of pore diameter distribution is larger in shales, gas flow in shales undergoes more complex flow regimes, and the permeability correction factor differs a lot.

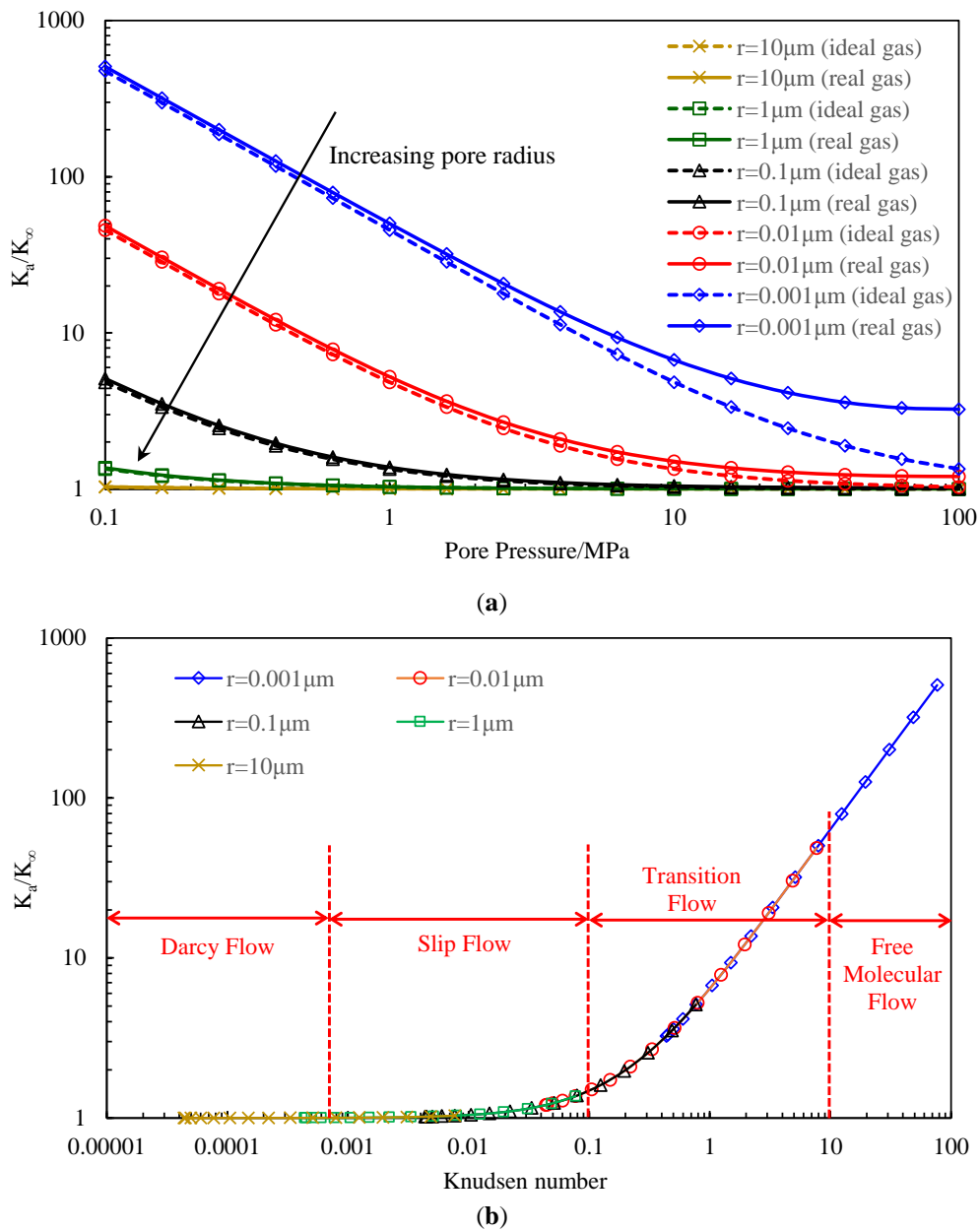


Figure 4. Permeability correction factor for methane at different pore radii. (a) Permeability correction factor versus pressure; (b) permeability correction factor versus Knudsen number.

The intrinsic permeability is expressed as [31]:

$$K_{\infty} = \frac{\phi}{\tau} \frac{r^2}{8} \tag{16}$$

Shale has a wide pore size distribution, and pores with different diameters contribute differently to apparent permeability. The intrinsic permeability of shales with wide pore diameter distribution can be calculated by the following equation [32,33]:

$$K_{\infty} = \frac{\phi}{\tau} \sum_{i=1}^N \frac{r_i^2}{8} \xi_i(r_i) \tag{17}$$

where it is assumed there are N types of pore diameter, $\xi_i(r_i)$ is the porosity distribution frequency when pore radius is equal to r_i . The pore size distribution is detected by nuclear magnetic resonance technique, which shows that the pore diameter ranges from 1 nm to 700 nm with a peak about 7 nm (Figure 5).

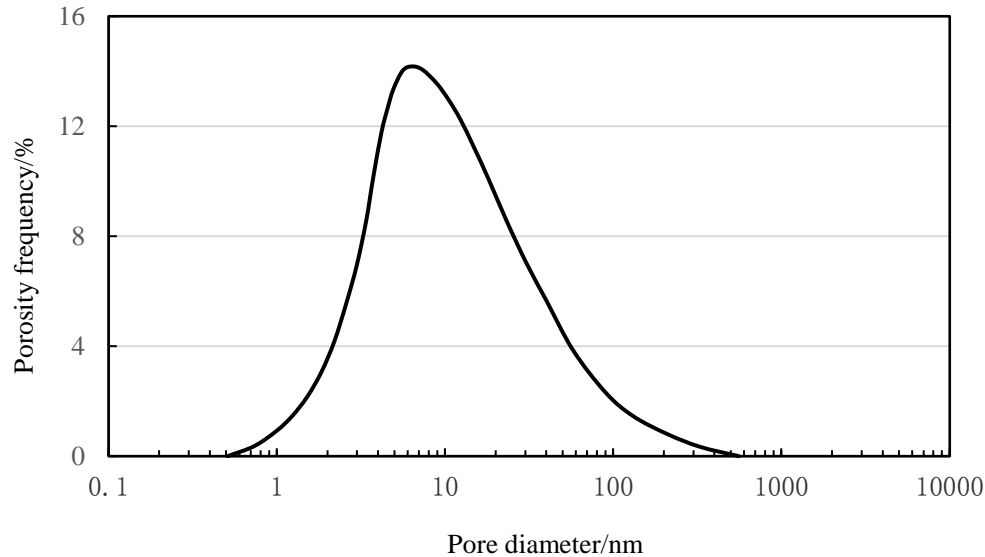


Figure 5. Pore size distribution of a Longmaxi Formation sample [33].

Considering pore with different diameters, the apparent permeability can be corrected by the frequency distribution of pores:

$$K_a = \frac{\phi}{\tau} \sum_{i=1}^N \left\{ \left[1 + \alpha_r \left(\frac{\mu_r}{p_g r_h} \sqrt{\frac{\pi ZRT}{2M}} \right) \frac{\mu_r}{p_g r_h} \sqrt{\frac{\pi ZRT}{2M}} \right] \left(1 + \frac{4 \frac{\mu_r}{p_g r_h} \sqrt{\frac{\pi ZRT}{2M}}}{1 - b \frac{\mu_r}{p_g r_h} \sqrt{\frac{\pi ZRT}{2M}}} \right) \frac{r_i^2}{8} \right\} \xi_i(r_i) \quad (18)$$

The permeability correction factor is:

$$f(Kn_r) = \frac{\sum_{i=1}^N \left\{ \left[1 + \alpha_r \left(\frac{\mu_r}{p_g r_h} \sqrt{\frac{\pi ZRT}{2M}} \right) \frac{\mu_r}{p_g r_h} \sqrt{\frac{\pi ZRT}{2M}} \right] \left(1 + \frac{4 \frac{\mu_r}{p_g r_h} \sqrt{\frac{\pi ZRT}{2M}}}{1 - b \frac{\mu_r}{p_g r_h} \sqrt{\frac{\pi ZRT}{2M}}} \right) \frac{r_i^2}{8} \right\} \xi_i(r_i)}{\sum_{i=1}^N \frac{r_i^2}{8} \xi_i(r_i)} \quad (19)$$

4. Gas and Water Transport Model in Multi-Scale Shale Gas Reservoirs

4.1. Gas Flow in Multiscale Shale Gas Reservoirs

In order to deduce and develop the seepage equations for shale gas reservoirs, some assumptions have been made, including isothermal reservoir, non-Darcy flow in shales and Darcy flow in hydraulic fractures as well as adsorbed gas only desorbing from the pore walls within shales.

Based on the above assumptions, the material balance equations for shale gas reservoirs are derived as follows according to the law of conservation of matter:

4.1.1. Gas Flow in Multiscale Shales

Mass balance equation for gas flow in multiscale shales per unit time per bulk volume of shale can be derived, which considers adsorbed gas on pore walls, multi-scale flow regimes in shales and the anisotropy of reservoirs:

$$\nabla \cdot \left[\frac{\vec{K}k_{rg}}{B_g\mu_g} (\nabla p_g - \rho_g g \nabla D) \right] - q_g = \frac{\partial}{\partial t} \left(\frac{\phi s_g}{B_g} + \rho_{bi} \frac{V_L p_g}{p_L + p_g} \right) \quad (20)$$

The adsorbed gas can be calculated by Langmuir isotherm equation:

$$V_a = \frac{V_L p_g}{p_L + p_g} \quad (21)$$

Taking Equation (19) into Equation (20), we can get the governing equation of gas phase:

$$\nabla \cdot \left[\frac{\vec{K}_{\infty} f(Kn_r) k_{rg}}{B_g \mu_g} (\nabla p_g - \rho_g g \nabla D) \right] - q_g = \frac{\partial}{\partial t} \left(\frac{\phi s_g}{B_g} + \rho_{bi} \frac{V_L p_g}{p_L + p_g} \right) \quad (22)$$

where $f(Kn_r)$ in Equation (22) can be calculated by Equation (19), which is used to correct the apparent permeability of shales caused by the submicron effects in pores with different diameters.

The permeability of the anisotropic shale gas reservoir \vec{K}_{∞} in Equation (22) can be derived from Equation (5):

$$\vec{K}_{\infty} = (k_{x\infty}, k_{y\infty}, k_{z\infty}) = (k_{\delta x\infty}, k_{\delta y\infty}, k_{\delta z\infty}) \begin{bmatrix} \cos^2 \alpha \cos^2 \beta & \cos^2 \alpha \sin^2 \beta & \sin^2 \alpha \\ \sin^2 \beta & \cos^2 \beta & 0 \\ \sin^2 \alpha \cos^2 \beta & \sin^2 \alpha \sin^2 \beta & \cos^2 \alpha \end{bmatrix} \quad (23)$$

4.1.2. Gas Flow in Hydraulic Fracture

Experimental results indicate that effective conductivity of both propped and unpropped fractures decreases with the decrease of effective stress [34]. According to the experimental results of Zhang et al. [35], the relationship between the effective permeability and gas pressure can be written as:

$$K_H = K_{H0} \cdot e^{-\alpha_s(p_{gi} - p_g)} \quad (24)$$

By applying the theory of equivalent fracture conductivity, the permeability of hydraulic fracture considering the stress-dependence effect can be calculated by [34]:

$$K_{eH} = \frac{K_H \cdot w_H}{\Delta x_H} = \frac{K_{Hi} \cdot w_H}{\Delta x_H} \cdot e^{-\alpha_s(p_{gi} - p_g)} \quad (25)$$

Gas flow in hydraulic fracture can be described by Darcy equation, so the following equation is obtained:

$$-\nabla p_g = \frac{\mu}{K_{eH} k_{rg}} v_g \quad (26)$$

4.2. Water Flow in Multiscale Shale Gas Reservoirs

4.2.1. Water Flow in Multiscale Shales

Mass balance equation for water flow in shale gas reservoirs per unit time per bulk volume of shale is:

$$\nabla \cdot \left[\frac{\overrightarrow{K}k_{rw}}{B_w\mu_w} (\nabla p_w - \rho_w g \nabla D) \right] - q_w = \frac{\partial}{\partial t} \left(\frac{\phi s_w}{B_w} \right) \quad (27)$$

We can get the governing equation of water phase:

$$\nabla \cdot \left[\frac{\overrightarrow{K}_\infty k_{rw}}{B_w\mu_w} (\nabla p_w - \rho_w g \nabla D) \right] - q_w = \frac{\partial}{\partial t} \left(\frac{\phi s_w}{B_w} \right) \quad (28)$$

where $\overrightarrow{K}_\infty$ in Equation (28) can be calculated by Equation (23).

4.2.2. Water Flow in Hydraulic Fracture

Water flow in hydraulic fracture can be described by Darcy equation as well as gas flow in hydraulic fracture:

$$-\nabla p_w = \frac{\mu}{K_{eH}k_{rw}} v_w \quad (29)$$

4.3. Validation of the Developed Numerical Model

A multi-stage fractured horizontal well in three-dimensional shale gas reservoir (Figure 6) is made to characterize and simulate gas flow from multiscale shales to hydraulic fractures. The dimension of the reservoir is $1136 \times 280 \times 50$ m, and the grid size is $139 \times 29 \times 1$ in the x , y , and z direction.

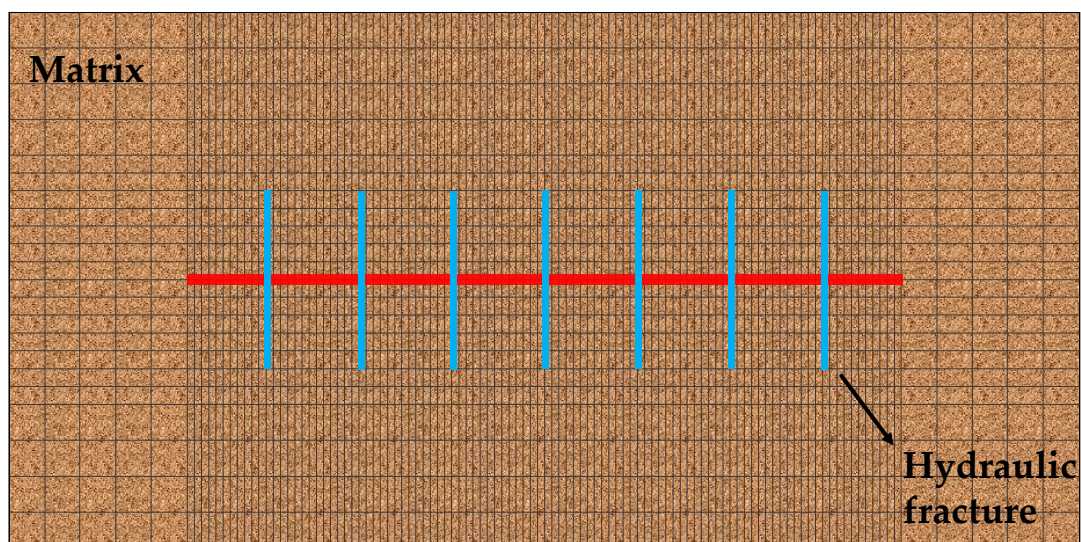
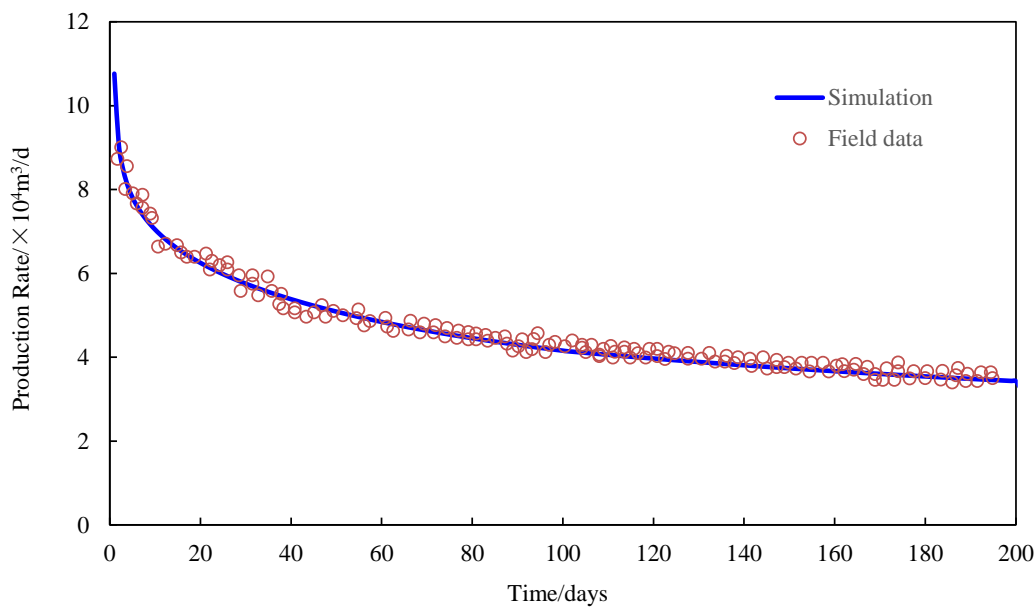


Figure 6. Schematic of fractured horizontal well in shale gas reservoir.

To examine the accuracy of the simulator formulations, the production data of the Marcellus shale is used in this paper. The parameters used for simulation are shown in Table 2. The reservoir parameters are dependent on the literature [36], and the adsorption parameters of Marcellus shale are obtained in literature [37]. The simulated gas production rate is proved to match well with the field data, which is shown in Figure 7. Therefore, the validity of this model is approved.

Table 2. Basic parameters for the numerical simulation.

Parameter	Value	Unit
Formation depth	2400	m
Formation thickness	50	m
Initial pressure	32.0	MPa
Initial temperature	355	K
Shale porosity	0.065	/
Shale permeability	6.0×10^{-4}	$10^{-3} \mu\text{m}^2$
Initial density of rock	2460	kg/m^3
Langmuir pressure	3.44	MPa
Langmuir volume	5.66	cm^3/g
Initial gas saturation	0.75	/
Gas specific gravity	0.58	/
Horizontal well length	640	m
Hydraulic fracture spacing	87	m
Half-length of hydraulic fracture	68	m
Number of hydraulic fractures	7	/
Stress-sensitivity coefficient	1.5×10^{-8}	Pa^{-1}
Wellbore pressure	6	MPa
Wellbore radius	0.1	m

**Figure 7.** The match result of gas production rate for shale gas reservoirs with field date.

5. Results and Discussion

According to the validated simulator for shale gas reservoirs, the effects of anisotropy permeability, non-Darcy flow in multiscale shales and gas-water flow on production rate as well as cumulative production of multi-stage fractured horizontal well are analyzed thoroughly.

5.1. Effect of Permeability Anisotropy on Production Rate

We assume that maximum permeability is five times larger than minimum permeability parallel to bedding, and permeability parallel to bedding (red arrows in Figure 8) is 10 times larger than permeability perpendicular to bedding, since Kwon et al. [4] proposed that permeabilities (Wilcox shale) measured parallel to bedding are about 1 order of magnitude greater than permeability measured perpendicular to bedding.

Effect of dip (the angle between the bedding plane of shales and the horizontal plane) on gas production rate and cumulative production has been shown in Figure 9. We can find that the greater the dip is, the faster the production rate declines, and the more the cumulative production decreases. When dip becomes bigger, it is easier for gas flow in the vertical direction (Figure 8d) which is useless to improve the performance of fractured horizontal well owing to the vertical hydraulic fractures. The dip has a greater impact on production rate and cumulative production than azimuth (Figure 10), and production rate and cumulative production increase with the decrease of azimuth. A smaller azimuth facilitates gas flowing towards the vertical hydraulic fractures of fractured horizontal well (the direction of horizontal well is assumed to be parallel with the maximum permeability when azimuth is equal to 0°).

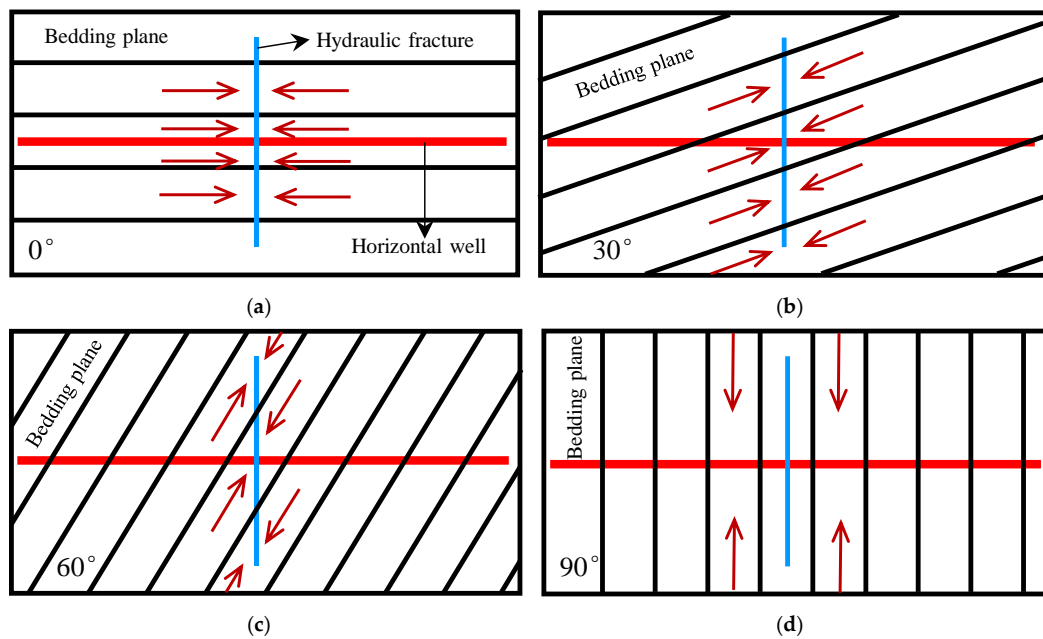


Figure 8. Fractured horizontal well at different angles to bedding plane of shale gas reservoir (a) dip of 0°; (b) dip of 30°; (c) dip of 60°; (d) dip of 90° (red arrows represent permeability parallel to bedding plane).

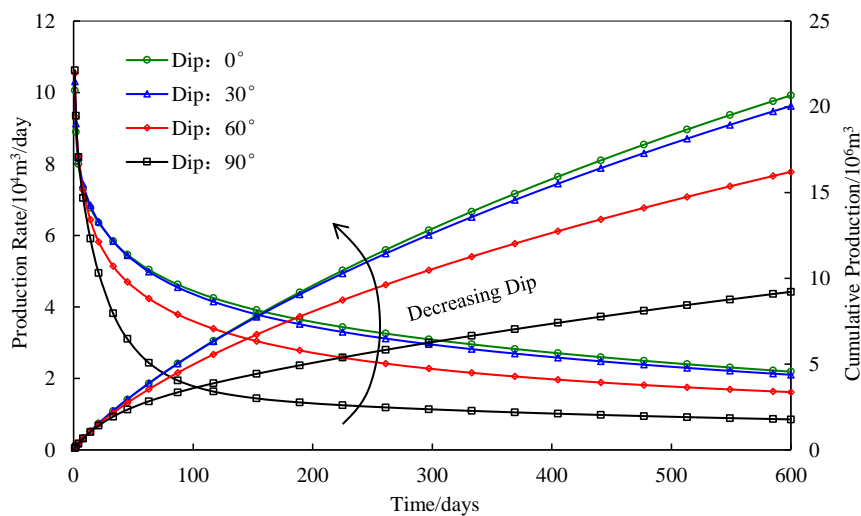


Figure 9. Effect of dip on gas production rate and cumulative production (decline curves represent gas production rate curves, increasing curves represent cumulative production curves).

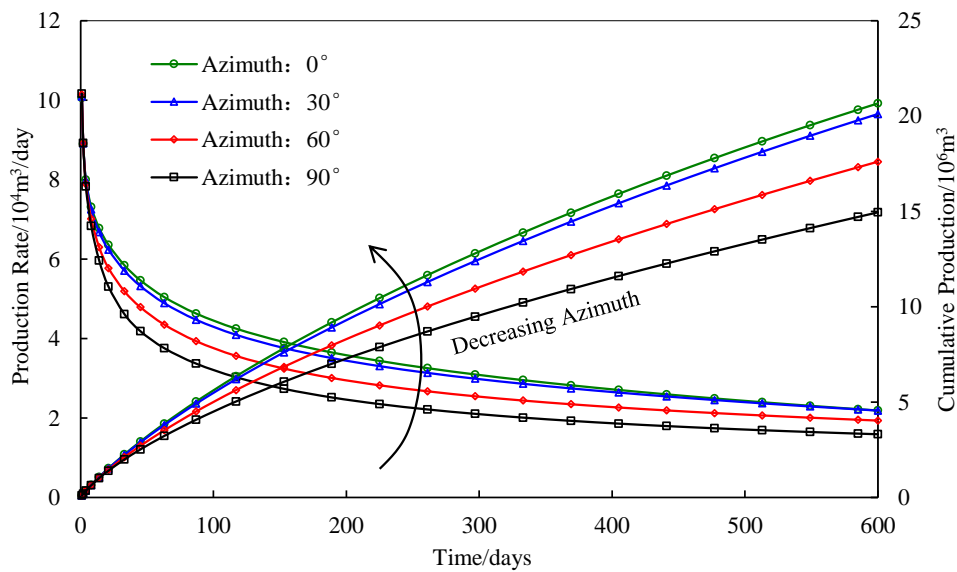


Figure 10. Effect of azimuth on gas production rate and cumulative production (decline curves represent gas production rate curves, increasing curves represent cumulative production curves).

Figure 11 presents the ratio of production at different dip (or azimuth) and production at dip (or azimuth) of 90° when fractured horizontal well produced after 600 days. We can find that the ratio decreases with the increase of the degrees of dip (or azimuth). The effects are small for angles less than 30° (Figure 8a), moderate for dip between 30° and 60° (Figure 8b,c) and large for dip greater than 60°. When dip increases to 90° (Figure 8d), the production becomes the lowest. This is because that permeabilities measured parallel to bedding are about one order of magnitude greater than those measured perpendicular to bedding according to the research of Kwon et al. [4]. Therefore, angles between the direction of horizontal well and bedding plane better be less than 30°. We can also find from Figure 11 that the effect of dip angle on production is greater than azimuth. Azimuth only affects permeability parallel to bedding, which is much greater than permeability perpendicular to bedding plane, so the production rate will not decline much when azimuth changes.

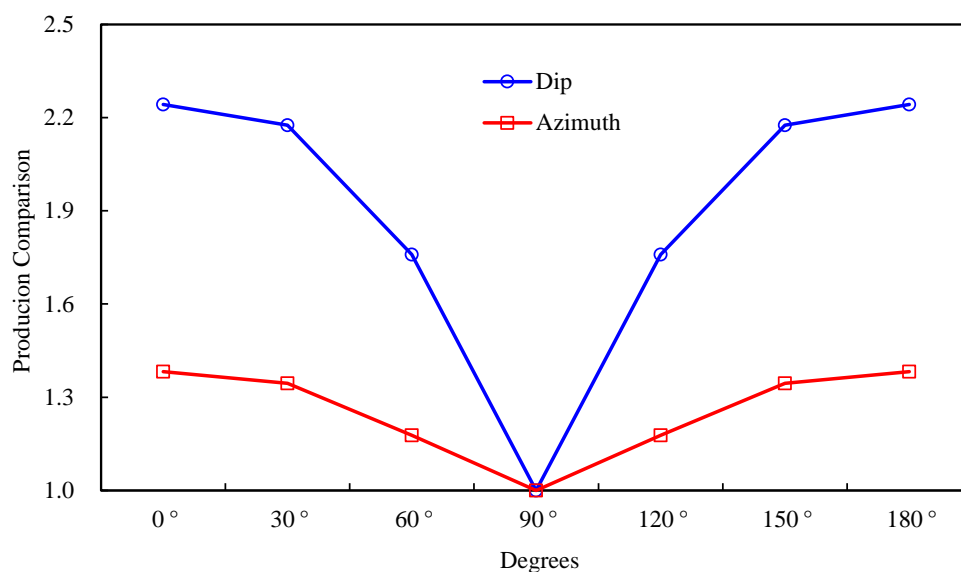


Figure 11. The ratio of production at different dip (or azimuth) and production at dip (or azimuth) of 90° when fractured horizontal well produced after 600 days.

5.2. Effects of Non-Darcy Effect in Multiscale Shales

According to the gas phase pressure of each grid block in shale gas reservoir (Figure 12a), we can calculate Knudsen number of every grid block in shale gas reservoir (Figure 12b) according to Equation (14), then classify flow regimes of gas flow in formation, and finally determine the permeability correction factor of each grid block in shale gas reservoirs according to Equation (19) (Figure 12c).

Figure 12a shows the distribution of gas phase pressure when shale permeability is equal to 6×10^{-4} mD and fractured well produced after 600 days. Figure 12b presents Knudsen number of each grid block in shale gas reservoirs after 600 days. We can conclude that the grid blocks get closer to hydraulic fractures, Knudsen number becomes bigger. Since Knudsen number is negatively correlated with pressure, Knudsen number increases with the decrease of pressure. The distribution of permeability correction factor is similar to Knudsen number (Figure 12c), and permeability correction factor increases with Knudsen number for the reason that permeability correction factor is positively related with Knudsen number according to Equation (9).

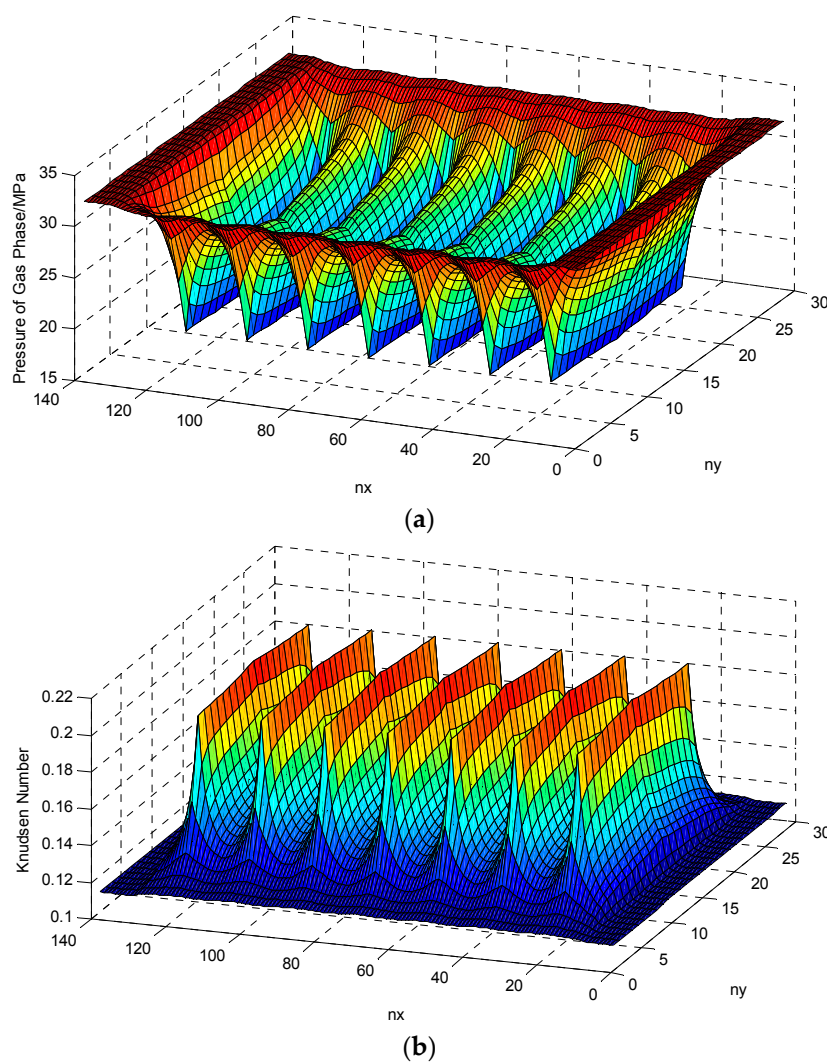


Figure 12. Cont.

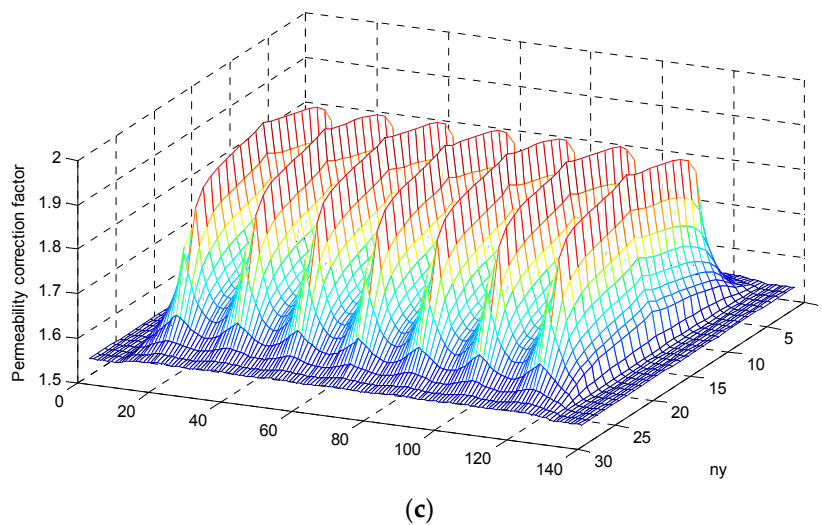


Figure 12. Distribution map of parameters in shale gas reservoir when K_{∞} equals 6×10^{-4} mD after 600 days (n_x and n_y represent the numbers of grid blocks in x direction and y direction respectively). (a) gas phase pressure; (b) Knudsen number; (c) permeability correction factor.

Figure 13 presents the gas production rate and cumulative production of a multi-fractured horizontal well under different shale permeabilities. It is shown that gas production rate and cumulative production both increase with the shale permeability. However, the increase of production rate and cumulative production which consider the non-Darcy flow effects in shales decreases with the increase of permeability of shales, compared with the production rate and cumulative production only considering Darcy flow or viscous flow. It means that the effects of non-Darcy flow on production rate and cumulative production become more significant as the permeability of shales gets lower.

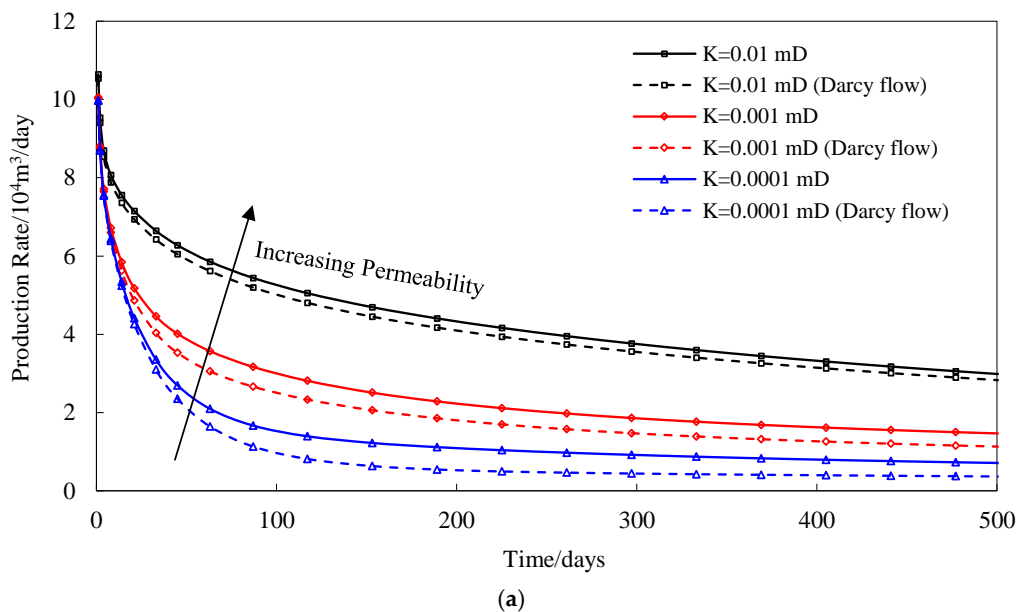


Figure 13. Cont.

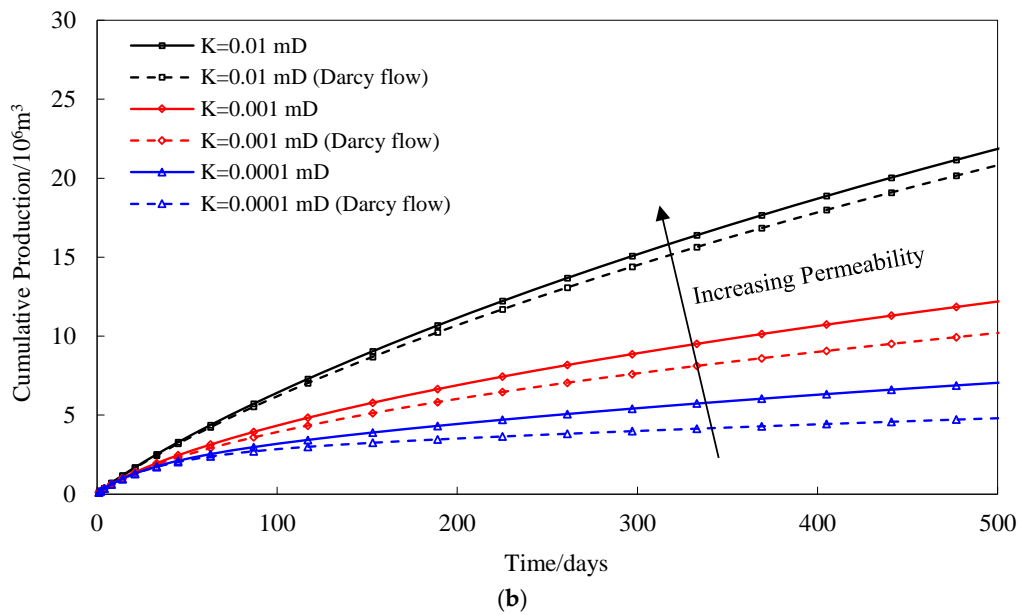


Figure 13. Effects of non-Darcy flow in multiscale shale matrix under different permeabilities of shales (solid lines in this figures represent gas production rate and cumulative production with considering the non-Darcy flow effects, dashed lines in this figure represent gas production rate and cumulative production only considering Darcy flow or viscous flow.) (a) Production rate under different shale permeabilities; (b) Cumulative production under different shale permeabilities.

5.3. Effect of Gas-Water Flow in Formation

The effect of initial water saturation on production rate and cumulative production of the multi-stage fractured horizontal well in shale gas reservoirs is shown in Figure 14. Bigger initial water saturation means less free gas stored in reservoirs, so production rate declines a lot at the early period of exploitation as initial water saturation increases. Moreover, bigger water saturation causes a lower relative permeability of gas phase, which is not favorable for gas flow in reservoirs as well.

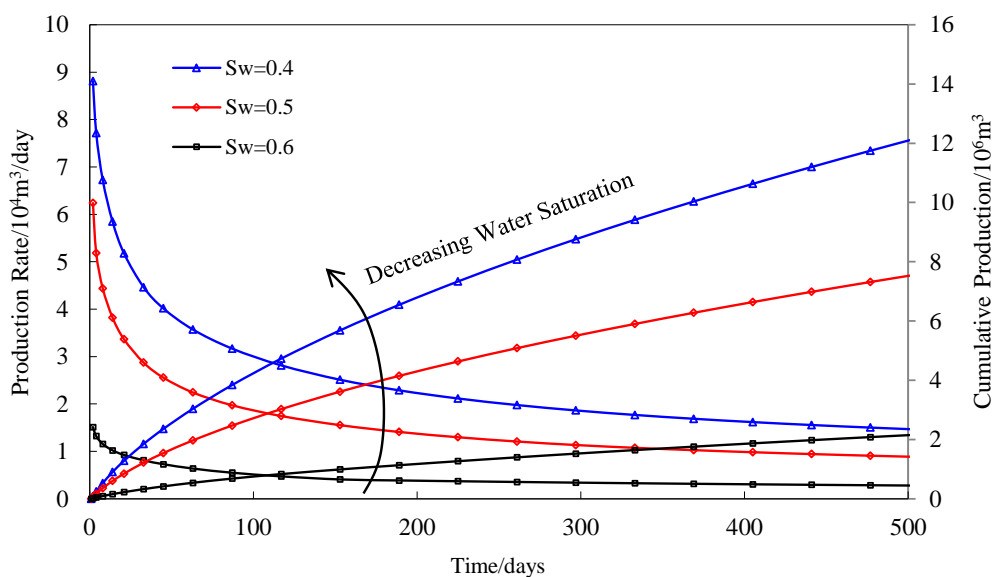


Figure 14. Effect of initial water saturation on gas production rate and cumulative production (decline curves represent gas production rate curves, increasing curves represent cumulative production curves).

Figure 15 shows the relative permeability curves with different nanopore radii which was proposed by Li et al. [38], and Figure 16 illustrates the effect of relative permeability on gas production rate and cumulative production. Production rates are the same at the early period, and then the production rate declines faster as the relative permeability decreases (nanopore radius decreases). This is because that the initial gas and water stored in reservoirs is not changed, but the gas production rate will decline as the decrease of relative permeability of gas phase.

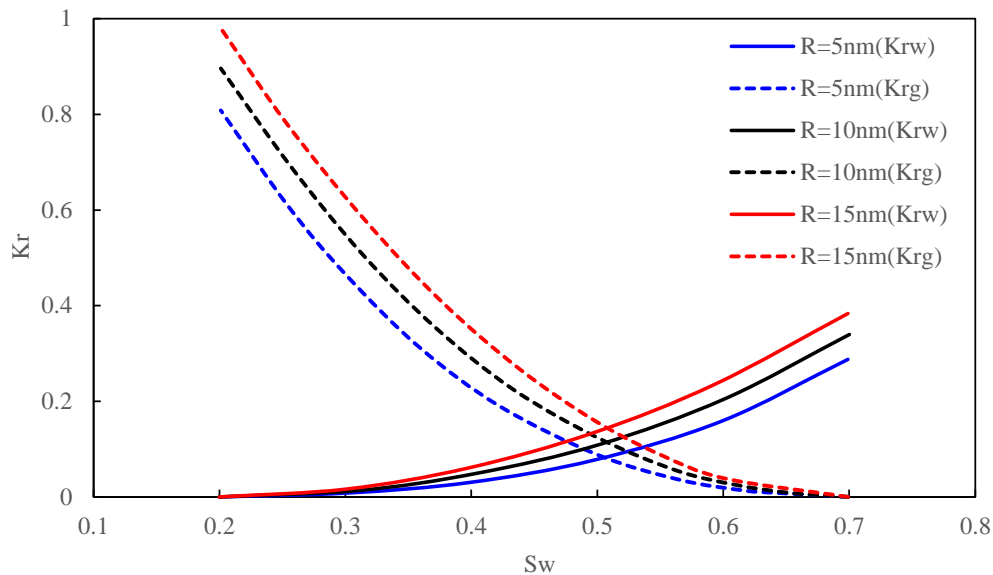


Figure 15. Relative permeability curves with different nanopore radii R [38].

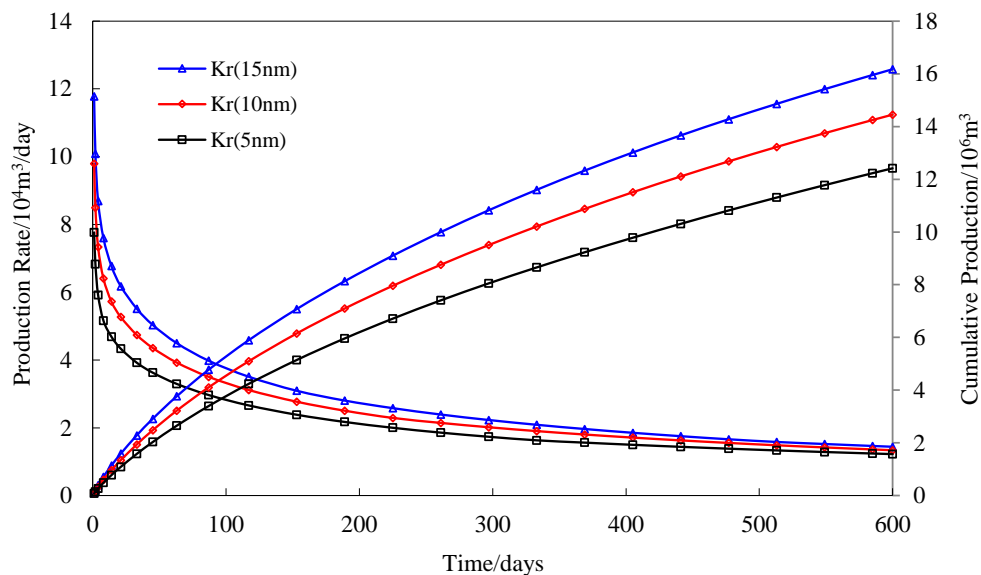


Figure 16. Effect of relative permeability on gas production rate and cumulative production (decline curves represent gas production rate curves, increasing curves represent cumulative production curves).

6. Conclusions

This paper presents a three dimensional numerical model which is valid for the entire Knudsen’s range (continuum flow, slip flow, transition flow and free molecular flow) in shale gas reservoirs, and the effects of permeability anisotropy, gas-water flow and the simulation of hydraulic fracturing cracks

were taken into consideration. The simulation result was validated with field data, and the influencing parameters has been analyzed thoroughly. The following conclusions can be drawn:

1. A new model of permeability anisotropy for shale gas reservoirs is presented to calculate permeability in an arbitrary direction in three dimensional space, and a numerical model which is valid for all flow regimes in multiscale shale gas reservoirs was developed. The simulation result showed that numerical model matches well with the field data of the Marcellus shale.
2. The production rate and cumulative production increase with the decrease of dip and azimuth (supposing that the direction of horizontal well is parallel with the maximum permeability when azimuth is equal to 0°), but dip has a greater impact on production rate and cumulative production than azimuth. The effects of dip (azimuth) on production are small for angles less than 30° , moderate for dip (azimuth) between 30° and 60° , and large for dip (azimuth) greater than 60° . When dip (azimuth) increases to 90° , the production becomes the lowest.
3. Different flow regimes in this three dimensional numerical model were classified by Knudsen number, and the effect of non-Darcy in multiscale shales on production rate was emphatically analyzed under different permeabilities of shales. The production rate of multi-stage fractured horizontal well increases with the permeability of shale. But the increase of gas production which considers the effects of non-Darcy flow in multiscale shales decreases with the increase of shale permeability, compared with the gas production rate only considering viscous flow.
4. The effect of gas-water flow on the performance of multi-stage fractured horizontal wells was analyzed as well. Initial water saturation has a greater impact on gas production than relative permeability curves with different nanopore radii, and initial water saturation affects the production throughout the whole development process of shale gas reservoirs.

Acknowledgments: The authors would like to thank Hubei Cooperative Innovation Center of Unconventional Oil and Gas for supporting our work. This project was partly supported by National Natural Science Foundation of China (Grant No. 51704032). The authors would like to acknowledge the financial support of Hubei Provincial Department of Education (Grant No. Q20171303) and Science and Technology Department of Hubei Province (Grant No. 2017CFB146).

Author Contributions: Ting Huang and Zhengwu Tao proposed the original idea for this paper. The numerical simulation was done by Erpeng Li and Qiqi Lyu, and the work was supervised by Xiao Guo. This paper was written by Ting Huang and modified by Zhengwu Tao.

Conflicts of Interest: The authors declare no conflict of interest.

Nomenclature

Latin

A_1	fitting adjustable coefficient, 7.9 [30]
A_2	fitting adjustable coefficient, 9.0×10^{-6} [30]
A_3	fitting adjustable coefficient, 0.28 [30]
b	slippage coefficient
B_g	gas volume factor
B_w	water volume factor
$f(Kn)$	permeability correction factor
g	gravitational acceleration, m/s^2
i, j, k	coordinates of grid block
K_a	apparent permeability
K_H	permeability of hydraulic fracture
K_{H0}	initial permeability of hydraulic fracture
K_∞	absolute permeability
k_B	Boltzmann Constant, 1.3805×10^{-23} J/K

k_{rg}	relative permeability of gas phase
k_{rw}	relative permeability of water phase
$k_{\delta x}$	maximum permeability measured parallel to bedding plane
$k_{\delta y}$	minimum permeability measured parallel to bedding plane
$k_{\delta z}$	permeability measured perpendicular to bedding plane
k_n	permeability in an arbitrary direction
Kn	Knudsen number
M	molecular mass, kg/mol
p	pressure, Pa
p_g	pressure of gas phase, Pa
p_{gi}	initial pressure of gas phase, Pa
p_L	Langmuir's pressure, Pa
p_c	critical pressure of methane, 4.5992×10^6 Pa [30]
p_w	pressure of water phase, Pa
q_g	gas volume flux per unit volume of shale and per unit time
q_w	water volume flux per unit volume of shale and per unit time
r	pore radius
r_h	equivalent hydraulic radius of pores
r_w	wellbore radius
s_g	gas saturation
s_w	water saturation
T	temperature at formation condition, K
T_c	critical temperature of methane, 190.564K [30]
v_g	gas flow rate, m/s
v_w	water flow rate, m/s
V_a	volume of adsorbed gas (standard condition) under formation pressure, m^3/kg
V_L	Langmuir's volume at standard condition, m^3/kg
w_H	width of hydraulic fracture
x, y, z	distance coordinates, m
Z	gas compressibility factor
<i>Greek letters</i>	
α	dip
α_r	rarefaction coefficient
α_s	stress-sensitivity coefficient, Pa^{-1}
β	azimuth
$\delta x, \delta y, \delta z$	directions of principal permeabilities
$\bar{\lambda}$	gas molecule mean free path, m
μ	viscosity, $Pa \cdot s$
μ_g	gas viscosity, $Pa \cdot s$
μ_w	water viscosity, $Pa \cdot s$
ρ_{bi}	bulk density of shale at initial reservoir pressure, kg/m^3
ρ_g	gas density, kg/m^3
ρ_w	water density, kg/m^3
σ	collision diameter of gas molecule
τ	tortuosity of shale
ϕ	porosity of shale

Appendix A. Derivation of Calculation Model of Permeability Anisotropy in Two Dimensional Space

As shown in Figure A1, the confused understandings in composition and decomposition of permeability vector are illustrated as follows:

- Vector composition: the reservoir is assumed to be homogeneous and isotropic, so the permeabilities in all directions are equal to k , while the permeability in the direction of k_3 should be according to the character of vector composition, which is contrary to the assumption that permeabilities in all directions should be k .

- (b) Vector decomposition: the reservoir is assumed to be homogeneous and isotropic, and the permeabilities in all directions are equal to k , while the permeability in the direction of k_ω should be $k \cdot \cos \alpha$ according to the character of vector decomposition, which is contrary to the assumption that permeabilities in all directions are equal to k .

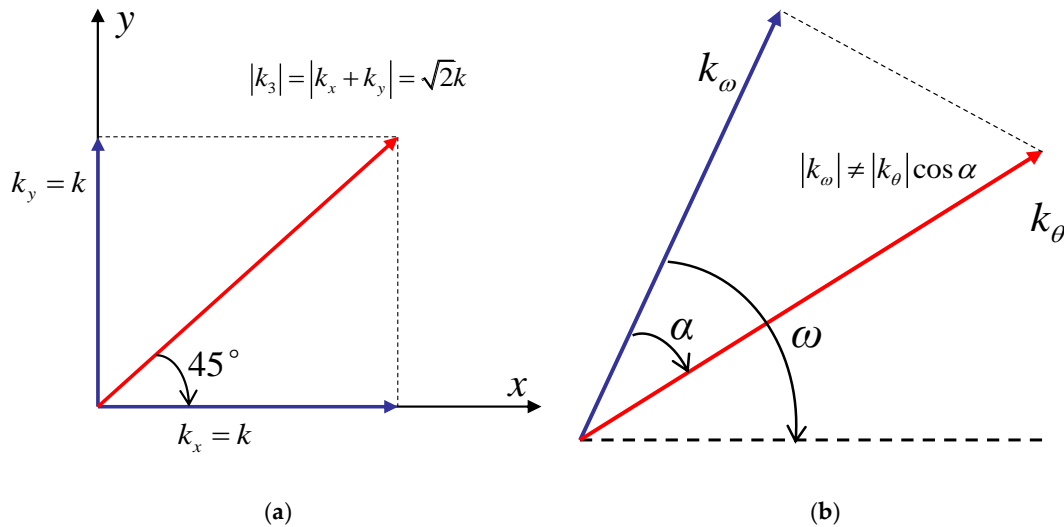


Figure A1. Schematic for incorrect composition and decomposition of permeability vector. (a) composition of permeability vector; (b) decomposition of permeability vector.

Thus, permeability cannot be composed according to the character of vector composition and decomposition. The relationship between permeability in an arbitrary direction (k_n), maximum permeability ($k_{\delta x}$) and minimum permeability ($k_{\delta y}$) in x - y axis (Figure A2) can be obtained through equivalent displacement principle, which was proposed by Wang et al. [39].

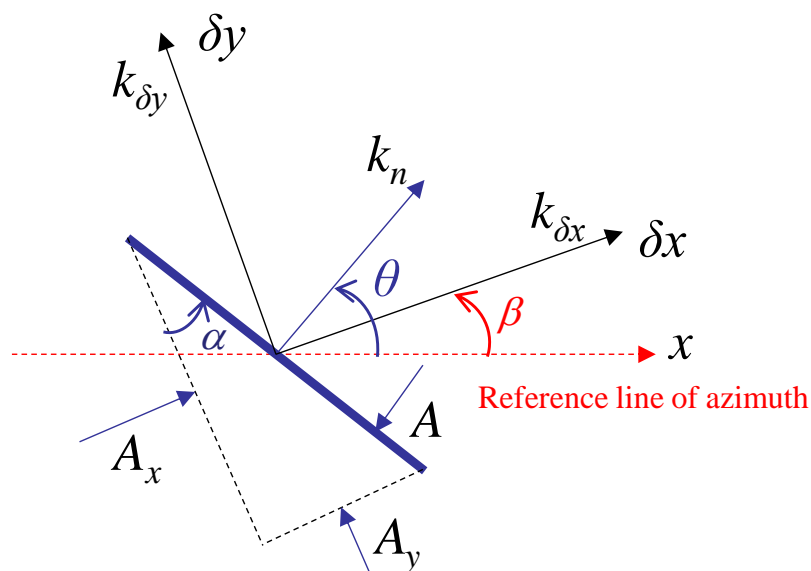


Figure A2. Schematic used to deduce the calculation model of permeability.

k_n is the permeability in n direction, v_n is the flow rate of n direction, μ is the viscosity, so we can write:

$$v_n = -\frac{k_n}{\mu} \nabla P_n \tag{A1}$$

Flow flux through seepage section A is:

$$Q_n = Av_n = -A \frac{k_n}{\mu} \nabla P_n \quad (\text{A2})$$

A_x is the effective seepage area of section A in the δx direction, β is the azimuth of $k_{\delta x}$, θ is the azimuth of k_n , so the relationship among α , β , and θ is:

$$\alpha = \theta - \beta \quad (\text{A3})$$

so we can get the relationship between A_x and A :

$$A_x = A \cos \alpha = A \cos(\theta - \beta) \quad (\text{A4})$$

The effective seepage area of section A in the δy direction is:

$$A_y = A \sin \alpha = A \sin(\theta - \beta) \quad (\text{A5})$$

The component of ∇P_n in the δx direction is:

$$\nabla P_{nx} = \nabla P_n \cos(\theta - \beta) \quad (\text{A6})$$

The flow flux through section A along δx direction under the action of ∇P_{nx} is:

$$Q_x = -A_x \frac{k_{\delta x}}{\mu} \nabla P_{nx} = -A \frac{k_{\delta x}}{\mu} \nabla P_n \cos^2(\theta - \beta) \quad (\text{A7})$$

We can get the flow flux through section A along δy direction in the same way:

$$Q_y = -A_y \frac{k_{\delta y}}{\mu} \nabla P_{ny} = -A \frac{k_{\delta y}}{\mu} \nabla P_n \sin^2(\theta - \beta) \quad (\text{A8})$$

The flow flux through section A (Q_n) is the sum of Q_x and Q_y . By combining with Equation (A2), Equations (A7) and (A8), we can obtain:

$$k_n = k_{\delta x} \cos^2(\theta - \beta) + k_{\delta y} \sin^2(\theta - \beta) \quad (\text{A9})$$

As the maximum permeability ($k_{\delta x}$) and minimum permeability ($k_{\delta y}$) can be tested in laboratory, the permeability in x direction and y direction can be calculated according to Equation (A9):

$$k_x = k_{\delta x} \cos^2 \beta + k_{\delta y} \sin^2 \beta \quad (\theta = 0^\circ) \quad (\text{A10})$$

$$k_y = k_{\delta x} \sin^2 \beta + k_{\delta y} \cos^2 \beta \quad (\theta = 90^\circ) \quad (\text{A11})$$

References

1. Davis, R.A. *Depositional Systems: An Introduction to Sedimentology and Stratigraphy*, 2nd ed.; Prentice Hall: Upper Saddle River, NJ, USA, 1992.
2. Deng, J.; Zhu, W.; Ma, Q. A new seepage model for shale gas reservoir and productivity analysis of fractured well. *Fuel* **2014**, *124*, 232–240. [[CrossRef](#)]
3. Young, A.; Low, P.F.; McLatchie, A.S. Permeability studies of argillaceous rocks. *J. Geophys. Res.* **1964**, *69*, 4237–4245. [[CrossRef](#)]
4. Kwon, O.; Kronenberg, A.K.; Gangi, A.F.; Johnson, B.; Herbert, B.E. Permeability of illite-bearing shale: 1. Anisotropy and effects of clay content and loading. *J. Geophys. Res.* **2004**, *109*, B10205. [[CrossRef](#)]
5. Chemali, R.; Gianzero, S.; Su, S.M. The effect of shale anisotropy on focused resistivity Devices. In Proceedings of the SPWLA 28th Annual Logging Symposium, London, UK, 29 June–2 July 1987.
6. Johnston, J.E.; Christensen, N.I. Seismic anisotropy of shales. *J. Geophys. Res.* **1995**, *100*, 5991–6003. [[CrossRef](#)]
7. Safdar, K.; Sajjad, A.; Han, H. Importance of shale anisotropy in estimating insitu stresses and wellbore stability analysis in Horn river basin. In Proceedings of the Canadian Unconventional Resources Conference, Calgary, AB, Canada, 15–17 November 2011.

8. Kocks, U.F.; Tome, C.N.; Wenk, H.R. *Texture and Anisotropy: Preferred Orientations in Polycrystals and Their Effect on Materials Properties*; Cambridge University: Cambridge, UK, 1998.
9. Wenk, H.R.; Voltolini, M.; Mazurek, M.; Van Loon, L.R.; Vinsot, A. Preferred orientations in shales: Callvovo-oxfordian shale (France) and opalinus clay (Switzerland). *Clays Clay Min.* **2008**, *56*, 285–306. [[CrossRef](#)]
10. Roy, S.; Raju, R. Modeling gas flow through microchannels and nanopores. *J. Appl. Phys.* **2003**, *93*, 4870–4879. [[CrossRef](#)]
11. Wu, K.; Chen, Z.; Li, X. A model for multiple transport mechanisms through nanopores of shale gas reservoirs with real gas effect–adsorption-mechanic coupling. *Int. J. Heat Mass Transf.* **2016**, *93*, 408–426. [[CrossRef](#)]
12. Wu, K.; Li, X.; Guo, C.; Wang, C.; Chen, Z. A unified model for gas transfer in nanopores of shale-gas reservoirs: coupling pore diffusion and surface diffusion. *SPE J.* **2016**, *21*, 1583–1611. [[CrossRef](#)]
13. Javadpour, F. Nanopores and apparent permeability of gas flow in mudrocks (shales and siltstone). *J. Can. Pet. Technol.* **2009**, *48*, 16–21. [[CrossRef](#)]
14. Ozkan, E.; Raghavan, R.S.; Apaydin, O.G. Modeling of fluid transfer from shale matrix to fracture network. In Proceedings of the SPE Annual Technical Conference and Exhibition, Florence, Italy, 19–22 September 2010.
15. Shabro, V.; Torres-Verdin, C.; Javadpour, F. Numerical simulation of shale-gas production: From pore-scale modeling of slip-flow, Knudsen diffusion and Langmuir desorption to reservoir modeling of compressible fluid. In Proceedings of the SPE North American Unconventional Gas Conference and Exhibition, Woodlands, TX, USA, 14–16 June 2011.
16. Swami, V.; Settari, A. A Pore Scale Gas Flow Model for Shale Gas Reservoir. In Proceedings of the Americas Unconventional Resources Conference, Pittsburgh, PA, USA, 5–7 June 2012.
17. Huang, T.; Guo, X.; Chen, F. Modeling transient flow behavior of a multiscale triple porosity model for shale gas reservoirs. *J. Nat. Gas Sci. Eng.* **2015**, *23*, 33–46. [[CrossRef](#)]
18. Ziarani, A.S.; Aguilera, R. Knudsen’s permeability correction for tight porous media. *Transp. Porous Media* **2012**, *91*, 239–260. [[CrossRef](#)]
19. Beskok, A.; Karniadakis, G. A model for flows in channels pipes, and ducts at micro and nanoscales. *Microsc. Thermophys. Eng.* **1999**, *3*, 43–77.
20. Civan, F.; Rai, C.S.; Sondergeld, C.H. Shale-gas permeability and diffusivity inferred by improved formulation of relevant retention and transport mechanisms. *Transp. Porous Media*. **2011**, *86*, 925–944. [[CrossRef](#)]
21. Wang, J.; Liu, H.; Wang, L. Apparent permeability for gas transport in nanopores of organic shale reservoirs including multiple effects. *Int. J. Coal Geol.* **2015**, *152*, 50–62. [[CrossRef](#)]
22. Yuan, Y.; Doonechaly, N.G.; Rahman, S. An analytical model of apparent gas permeability for tight porous media. *Transp. Porous Media* **2016**, *111*, 193–214. [[CrossRef](#)]
23. Brown, M.; Ozkan, E.; Raghavan, R.; Kazemi, H. Practical solutions for pressure-transient responses of fractured horizontal wells in unconventional shale reservoirs. *SPE Reserv. Eval. Eng.* **2011**, *14*, 663–676. [[CrossRef](#)]
24. Zhao, Y.; Zhang, L.; Zhao, J.; Luo, J.; Zhang, B. “Triple porosity” modeling of transient well test and rate decline analysis for multi-fractured horizontal well in shale gas reservoir. *J. Pet. Sci. Eng.* **2013**, *110*, 253–262. [[CrossRef](#)]
25. Wang, H.T. Performance of multiple fractured horizontal wells in shale gas reservoirs with consideration of multiple mechanisms. *J. Hydrol.* **2014**, *510*, 299–312. [[CrossRef](#)]
26. Cipolla, C.L.; Lolon, E.P.; Erdle, J.C.; Rubin, B. Reservoir modeling in shale-gas reservoirs. *SPE Reserv. Eval. Eng.* **2010**, *13*, 638–653. [[CrossRef](#)]
27. Clarkson, C.R.; Nobakht, M.; Kaviani, D.; Ertekin, T. Production analysis of tight-gas and shale-gas reservoirs using the dynamic-slippage concept. *SPE J.* **2012**, *17*, 230–242. [[CrossRef](#)]
28. Li, D.; Zhang, L.; Lu, D. Effect of distinguishing apparent permeability on flowing gas composition, composition change and composition derivative in tight-and shale-gas reservoir. *J. Pet. Sci. Eng.* **2015**, *128*, 107–114. [[CrossRef](#)]
29. Civan, F. Effective correlation of apparent gas permeability in tight porous media. *Transp. Porous Media* **2010**, *82*, 375–384. [[CrossRef](#)]

30. Wu, K.; Chen, Z.; Li, X. Flow behavior of gas confined in nanoporous shale at high pressure: Real gas effect. *Fuel* **2017**, *205*, 173–183. [[CrossRef](#)]
31. Florence, F.A.; Rushing, J.A.; Newsham, K.E.; Blaingame, T.A. Improved permeability prediction relations for low permeability sands. In Proceedings of the 2007 SPE Rocky Mountain Oil & Gas Technology Symposium, Denver, CO, USA, 16–18 April 2007.
32. Johnson, D.L.; Koplik, J.; Schwartz, L.M. New pore-size parameter characterizing transport in porous media. *Phys. Rev. Lett.* **1986**, *57*, 2564–2567. [[CrossRef](#)] [[PubMed](#)]
33. Chen, P.; Jiang, S.; Chen, Y. An apparent permeability model of shale gas under formation conditions. *J. Geophys. Eng.* **2017**, *14*, 833–840. [[CrossRef](#)]
34. Wang, J.; Luo, H.; Liu, H. An integrative model to simulate gas transport and production coupled with gas adsorption, non-Darcy flow, surface diffusion, and stress dependence in organic-shale reservoirs. *SPE J.* **2017**, *22*, 244–264. [[CrossRef](#)]
35. Zhang, J.; Kamenov, A.; Zhu, D.; Hill, A.D. Laboratory measurement of hydraulic fracture conductivities in the Barnett Shale. In Proceedings of the SPE Hydraulic Fracturing Technology Conference, The Woodlands, TX, USA, 4–6 February 2013.
36. Meyer, B.R.; Bazan, L.W.; Jacot, R.H. Optimization of multiple transverse hydraulic fractures in horizontal wellbores. In Proceedings of the SPE Unconventional Gas Conference, Pittsburgh, PA, USA, 23–25 February 2010.
37. Yu, W.; Sepehrnoori, K. Simulation of gas desorption and geomechanics effects for unconventional gas reservoirs. *Fuel* **2014**, *116*, 455–464. [[CrossRef](#)]
38. Li, T.; Song, H.; Wang, J. An analytical method for modeling and analysis gas-water relative permeability in nanoscale pores with interfacial effects. *Int. J. Coal Geol.* **2016**, *159*, 71–81. [[CrossRef](#)]
39. Wang, D.; Zhou, Y.; Ma, P.; Tian, T. Vector properties and calculation model for directional rock permeability. *Rock Soil Mech.* **2005**, *26*, 1294–1297.



© 2017 by the authors. Licensee MDPI, Basel, Switzerland. This article is an open access article distributed under the terms and conditions of the Creative Commons Attribution (CC BY) license (<http://creativecommons.org/licenses/by/4.0/>).